HAL
open science

The ability of precision hard turning to increase rolling contact fatigue life

Nabil Jouini, Philippe Revel, P.-E. Mazeran, Maxence Bigerelle

To cite this version:

Nabil Jouini, Philippe Revel, P.-E. Mazeran, Maxence Bigerelle. The ability of precision hard turning to increase rolling contact fatigue life. Tribology International, 2013, 59, pp.141-146. 10.1016/j.triboint.2012.07.010 . hal-03616155

HAL Id: hal-03616155

https://uphf.hal.science/hal-03616155v1

Submitted on 11 Apr 2024

HAL is a multi-disciplinary open access archive for the deposit and dissemination of scientific research documents, whether they are published or not. The documents may come from teaching and research institutions in France or abroad, or from public or private research centers.

L'archive ouverte pluridisciplinaire **HAL**, est destinée au dépôt et à la diffusion de documents scientifiques de niveau recherche, publiés ou non, émanant des établissements d'enseignement et de recherche français ou étrangers, des laboratoires publics ou privés.

The ability of precision hard turning to increase rolling contact fatigue life

N. Jouini [a,*], P. Revel [b], P.-E. Mazeran [b], M. Bigerelle [c]

[a] Laboratoire de Mécanique Matériaux et Procédés, ESSTT, 5, Avenue Taha Hussein, 1008, Tunis, Tunisia
[b] Laboratoire Roberval, UMR 6253, UTC/CNRS, Centre de Recherche de Royallieu, 60205 Compiègne, France
[c] Laboratoire TemPo/LAMIH UMR 8201, Université de Valenciennes et du Hainaut Cambrésis, Le Mont Houy, 59313 Valenciennes, France

Keywords:
Precision hard turning
Rolling contact fatigue
Roughness
Bearing steel

A B S T R A C T

In this paper, precision hard turning is proposed for the finishing of the AISI 52100 bearing components to improve rolling contact fatigue life. This finishing process induces a homogenous microstructure at surface and subsurface layers. Fatigue life tests performed on a twin-disk machine show that rolling contact fatigue life increases as R_a value decreases. The bearing components reached 0.32 million cycles for $R_a = 0.25$ μm and 5.2 million cycles for $R_a = 0.11$ μm. In comparison, the bearing components achieved 1.2 million cycles with grinding ($R_a = 0.2$ μm) and 3.2 million cycles with grinding followed by honing ($R_a = 0.05$ μm) respectively.

1. Introduction

Bearing steel components are widely used in heavy mechanical industry e.g. aerospace, automotive, etc. These components are subjected to severe operating conditions such as high loads, high speed, extreme temperatures and hostile environments. Thus, bearing steel such as AISI 52100 is thermally treated to achieve martensitic structure that enhances desired mechanical properties, fatigue strength and wear resistance. Then, it is finished in its hardened state by grinding process to achieve surface integrity. However, precision hard turning, defined as single point cutting of part with hardness of material in excess of 45 HRC under small feed rate and fine depth of cut conditions, has become an attractive alternative to grinding process [1]. It offers very substantial benefits with respect to grinding process such as environment-friendly, low surface roughness amplitude [2], capability to generate complex workpiece geometry and induces deep compressive residual stresses that often increase the fatigue life [3]. In literature, the rolling contact fatigue (RCF) life of bearing steel components is heavily influenced by the surface topography [4,5] as well as metallurgical and mechanical state of the subsurface layers [6].

The surface roughness in elastohydrodynamic lubrication contacts has a significant effect on the component life [7]. The presence of the roughness on the contact surfaces modifies the normal pressure distribution through local variations in the pressure distribution and perturbations in the elastohydrodynamic lubrication film thickness [8–10]. For example, Kumar et al. [11] have shown that the maximum pressure increases with roughness amplitude indicating that higher roughness heights lead to localized thinning of the lubricant film and these results were confirmed by simulation [12]. Studying sinusoidal surface roughness under starved conditions, Labiau et al. [13] show that starvation combined with surface roughness drastically reduces fatigue life and proposes an analytical model.

The fatigue life of bearings is determined by the detachment of material (spalling) following the initiation of cracks below the contact surface, spalling due to surface irregularities and due to the distress caused by surface roughness or inadequate lubrication [14–16]. In the case of hardened steel, fatigue origins have resulted in a preponderance of surface asperities [17,18]. Thus, roughness is considered as one of the main causes of crack initiation for hard steel components.

However, hard turning can introduce modifications within the surface layer of a workpiece. These modifications are metallurgical transformations as a result of intense, localized and rapid thermomechanical loading. The surface layer can show an extremely different structure from the bulk material due to the white layer formation that appears white in colour under an optical microscope after polishing and etching or featureless in a scanning electron microscope [19]. It is referred to as untempered martensite [20] and characterized by an increase in hardness than the bulk material [19–21]. The mechanism of white layer formation is attributed to severe plastic deformation, which produces a homogenous structure or one with a very fine grain size, and/or rapid heating and quenching, which results in phase transformation [20–22].

* Corresponding author. Tel.: +216 98644026.
E-mail address: nabil.jouini@gmail.com (N. Jouini).

The white layer induced by hard turning was detrimental to component fatigue life [2–23]. Indeed, the thicker the white layer, the shorter the RCF life [18]. However, despite white layer occurrence, hard turning provides greater fatigue life than grinding process [24,25]. This can be explained by the compressive residual stresses induced by hard turning.

In this study, at first, the microstructure analysis and mechanical behavior of the surface and sub-surface layers were carried out. Then, the effect of surface roughness amplitude, characterized by the R_a value, on rolling contact fatigue was studied. Finally, a comparative analysis between precision hard turning, grinding, and grinding followed by honing was performed.

2. Experimental work

2.1. Experimental set-up and machining tool

The machining tests were conducted on high precision turning machine, as shown in Fig. 1. This machine is a prototype lathe, designed by Snecma™ Motor, with T-slide architecture. The two slides-ways (*X*- and *Z*-axes) are guided by hydrostatic-bearings offering low friction, high stiffness and high damping, fixed on a massive granite block (1.5 t), itself resting on four self-levelling pneumatic isolators. The straightness of both slides is better than 0.3 μm over a displacement of 100 mm. The spindle is mounted axially to the *Z*-axis and an active magnetic bearing is adopted to achieve greater spindle dynamic stiffness. Due to the high accuracy needed along *X*- and *Z*-axes, ironless linear motors ILD 24-050 (ETEL™) are used for feed drive system. Each linear axis is operated by a position control system controlled using an incremental linear encoders LIP 401R (Heindenhain™) having 4 nm resolution. Displacements are controlled by a computer numerical control system with a powerful numerical card (Programmable Multi-Axis Controller: PMAC-Deltatau™).

The machining tests were performed under dry cutting conditions using c-BN cutting tool inserts (ISO code CNGA 120408 S01030 7025) manufactured by Sandvik™ Coromant. The inserts were mounted using a Coro torn RC rigid clamp system in the tool holder DCLN 2525M12 (ISO), providing the following angles: rake angle $\gamma_0 = -6^\circ$, inclination angle $\lambda_s = -6^\circ$, cutting edge angle $\chi_r = 95^\circ$, clearance angle $\alpha = 6^\circ$ and nose radius $r = 0.8$ mm.

In this work, AISI 52100 bearing steel rings thermally treated to an average hardness of $61^{\pm 1}$ HRC were used as workpiece material. The length of the ring was 14 mm with outer diameter of 70 mm and the inner diameter of 19 mm.

During machining tests, a 5 μm fine depth of cut and two different cutting conditions (cutting speed and feed rate) were used for each specimen. The cutting parameters for each specimen under investigation are listed in Table 1.

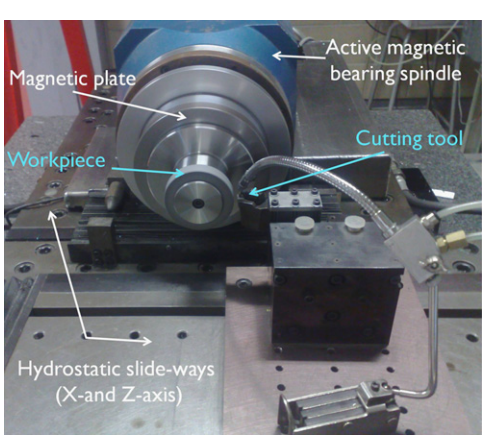

Fig. 1. Focus on the high precision turning machine used in this study.

Table 1
Cutting parameters of the specimens under investigation.

Cutting parameters	Specimens			
	1	2	3	4
Cutting speed, V_c (m/min)	210	210	260	360
Feed rate, f (μm/rev)	50	100	50	50
Depth of cut, DOC (μm)	5	5	5	5

2.2. Surface roughness measurement

The measurements were carried out by stylus profiler 3D KLA-Tencor™ (P-10 model) with a 2 μm tip radius, loaded with 50 mN. For each specimen, 25 roughness profiles were recorded perpendicular to the grooves. The scanning length and the sampling length were respectively 8 mm and 0.1 μm (80,000 data points along the profile length). Each profile was rectified by a third degree polynomial fit to remove the form of the surface. Then, the surface roughness amplitude (R_a) was computed.

2.3. Microstructure analysis

The cross-section of each specimen was prepared for microscopic analysis using traditional metallographic techniques. The specimens were carefully sectioned with an abrasive cutter, mounted in a thermosetting resin with carbon filler (PolyFast) for SEM examination, followed by gentle grinding and polishing with diamonds, successively using grain sizes of 6, 3 and 1 μm, then etched using a 2% Nital solution for approximately 10 s. The micrographic analyses of cross-sections were then carried out using scanning electron microscope (Philips XL30 ESEM-FEG).

2.4. Nanohardness measurement

The mechanical behavior was then investigated to reveal the difference between surface and sub-surface layers. The nanoindentation technique was used because it has been widely adopted and used in the mechanical behavior characterisation of the materials at small scales [26]. Nanoindentation tests were performed with MTS Nanoindenter XP using a Berkovich indenter. The load vs. penetration curves obtained during one cycle of loading and unloading were analyzed using Oliver and Pharr method [27] to measure indentation hardness, where contact stiffness is obtained by the initial slope of the unloading curve.

3. Results and discussion

3.1. Microstructure and nanohardness of surface and sub-surface layers

The Scanning Electron Microscopy (SEM) observations of the transversal cross-section of each specimen clearly revealed metallurgical transformations in the subsurface (see Fig. 2). This can be seen as an affected layer consisting of a fine white layer on the top surface, followed by an optical transition zone and then the bulk material.

Fig. 3 represents the relative thickness of the white layer in each specimen produced by precision hard turning. From Fig. 3, it can be evaluated that the white layer thickness resides below 1 μm and is statistically constant with a mean layer thickness of 0.7 μm. According to literature [19–28], the thickness of the white

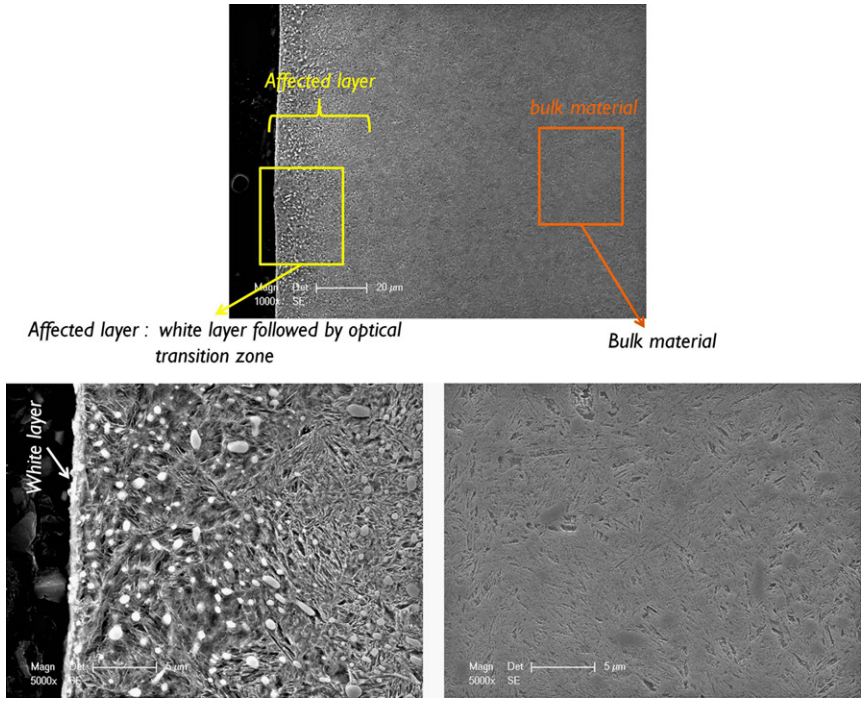

Fig. 2. Sub-surface microstructure relative to specimen 4.

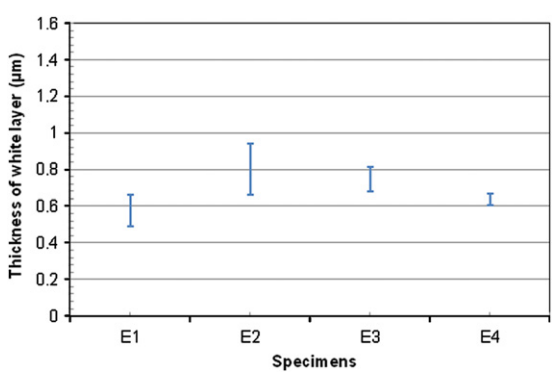

Fig. 3. Thickness evolution of the white layer.

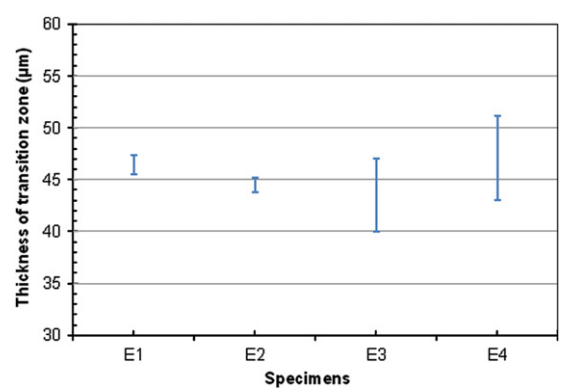

Fig. 4. Thickness evolution of the transition zone.

layer obtained during hard turning of AISI 52100 bearing steel should be between 3 and 50 µm. The values found in this study correspond only to a very fine thickness of white layer. This can be explained by the fine depth of cut (5 µm) used in this study. Beneath the white layer, the thickness of the transition zone is about 40–50 µm. It can be noted that this thickness is homogenous for all specimens (statically tested by analysis of variance), as shown in Fig. 4.

To summarize, these results show that precision hard turning generates both homogeneous thicknesses of the white layer and the transition zone. Thus, homogeneous microstructure is obtained at the surface and the subsurface layers whatever the cutting parameters under investigation.

To investigate the mechanical behavior of the white layer and the transition zone, a series of nanoindentation tests were carried out respectively on the top surface and the cross-sections of the machined samples.

Mechanical characterisation of the white layer: on the top surface, 15 nanoindentation tests were carried out according to 3×5 matrix of indentations with row and column spacing of 200 µm. Each test is a cyclic indentation test: loading–unloading–reloading, hence it results in 8 load vs. penetration curves which are obtained by varying the penetration depth on a total penetration depth of 2 µm. Thus, at each penetration depth, the hardness was calculated.

Mechanical characterisation of the transition zone: on the cross-section, 15 nanoindentation tests were carried out according to 3×5 matrix of indentations with row and column spacings of 100 and 20 µm, respectively. Each test is a classical indentation test: loading–unloading. The indentation matrix rows were created by carrying out the measurements at 20 and 40 µm in the transition zone whereas, at 60, 80 and 100 µm in the bulk material from the machined surface.

Due to the limited thickness of the white layer (< 1 µm), only 200 nm penetration depth measurements are reported here. The box-and-whisker plot shown in Fig. 5 illustrates the relative hardness of the white layer in the two specimens E1 and E3. From Fig. 5, the differences between the median hardness values do not exceed 0.5 GPa, that is not statistically significant. Thus, the homogeneous thickness evolution of the white layer revealed by SEM has a median hardness of 14 GPa. This hardness value

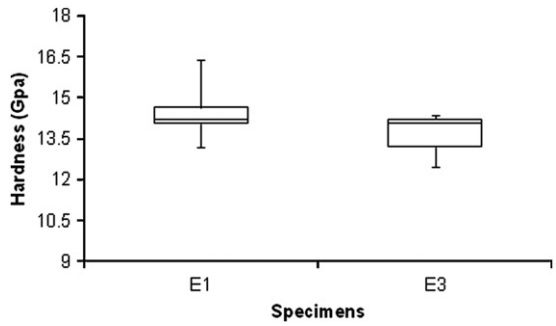

Fig. 5. Surface nanohardness (200 nm penetration depth).

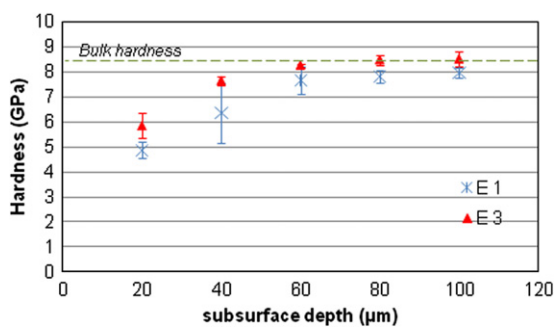

Fig. 6. Sub-surface nanohardness.

is about 50% higher than the hardness of the bulk material (8–9 GPa). While the microstructure of the bulk material is tempered martensite, the significantly higher value obtained for the nano-hardness of the white layer suggests that it is an untempered martensite.

Fig. 6 shows the hardness evolution as a function of subsurface depth. The results prove that the optical transition zone has a mean hardness of 5 GPa, which is about 30% softer than the bulk material. In this investigation there was no evidence of over-tempered martensite below the white layer.

3.2. Surface roughness

According to the previous study [29], an expert system [30,31] was used to quantify the relevancy of roughness parameters to characterize the functionalities of surfaces at all the scales including fractal aspect of the surface [32,33] for isotropic or anisotropic surface [34]. This system includes a recent powerful statistical technique called the bootstrap that was used by the authors to compute constitutive laws [35], fatigue life time prediction [36], adhesion properties of materials [37], etc. It was then found that the roughness amplitude R_a is considered as relevant roughness parameter to characterise the surface roughness obtained by precision hard turning with different cutting parameters. The R_a values of the four specimens investigated are summarized in Table 2. Under fine depth of cut of 5 µm, the results show that the feed rate strongly affects the R_a value. It has an increasing effect (from R_a=0.1 µm for specimen 1 to R_a=0.25 µm for specimen 2) for a cutting speed of 210 m/min. Indeed, it is well known that the theoretical value of the roughness amplitude R_a is primarily a function of feed rate for a given nose radius. Moreover, the optimal roughness amplitude R_a was obtained at a cutting speed of 210 m/min (specimen 1), which was considered as a high cutting speed in finish hard turning of AISI 52100, and also a very high cutting speed of 360 m/min (specimen 4).

Table 2
Surface roughness amplitude R_a.

Specimens	Cutting parameters			Surface roughness, R_a (µm)
	V_c (m/min)	f (µm/rev)	ap (µm)	
1	210	50	5	0.10
2	210	100	5	0.25
3	260	50	5	0.14
4	360	50	5	0.11

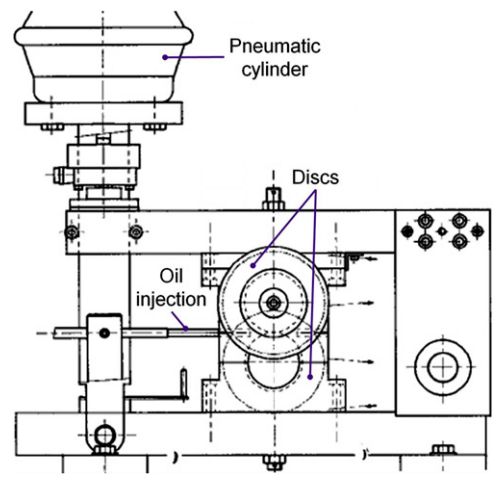

Fig. 7. Schematic view of twin-disc test rig.

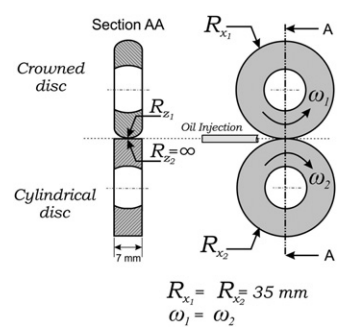

Fig. 8. Geometry of rolling contact fatigue test specimen.

4. Rolling contact fatigue test

4.1. Twin-disc test rig

RCF tests are performed on a twin-disc test rig (Fig. 7), specifically designed by CETIM to investigate the contact between gear teeth or ring and rolling elements. The two discs rolled under pure rolling conditions and lubricated by oil injection (Mobil Gear 629, kinematic viscosity of 15.8 cSt at 100 °C). The normal load is applied by a pneumatic cylinder. In the test rig, the lower disc is cylindrical (machined disc), while the upper disc is crowned (see Fig. 8). The geometry of the contact surfaces provides an elliptical contact area for applied load 1100 daN which corresponds to a Hertzian pressure of 3.8 GPa.

Two proximity Hall-effect sensors are used to detect initiate spalling on the surfaces. The test is stopped when one of the sensors detects a spalling or it reaches 10 million cycles. To evaluate the rolling contact fatigue life of precision hard turned, ground and ground followed by honed specimens, two tests were carried out on each specimen under the same conditions.

4.2. Surface spalling

Spalling is the predominant damage mechanism for the precision hard turned tested specimens. Fig. 9 shows a SEM image of a typical spall that was formed on the surface of precision hard turned specimen. Note that the damage mechanism is representative of all the test specimens. On an average, the width and the length of spalls are between 1 and 2 mm, and 2–4 mm respectively.

In order to determine the depth, and profile of spalls, the surface profilometer Dektak 150 from Veeco™ was used. Fig. 10 shows the 3D image of surface spall; the depth of the spall ranged from 250 to 350 μm.

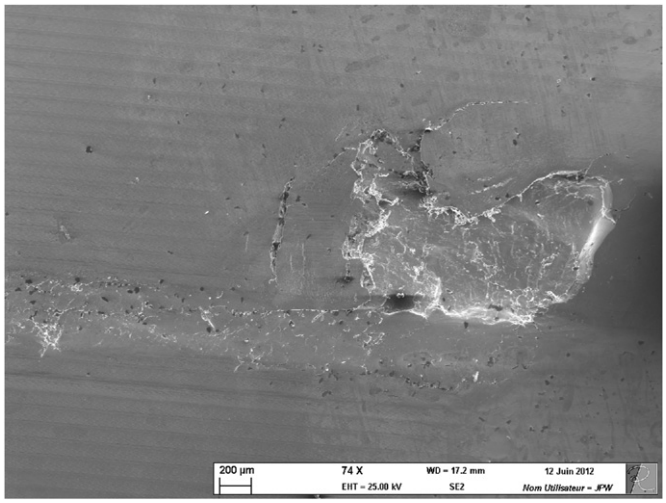

Fig. 9. SEM image of a spall formed on the surface of precision hard turned specimen 1.

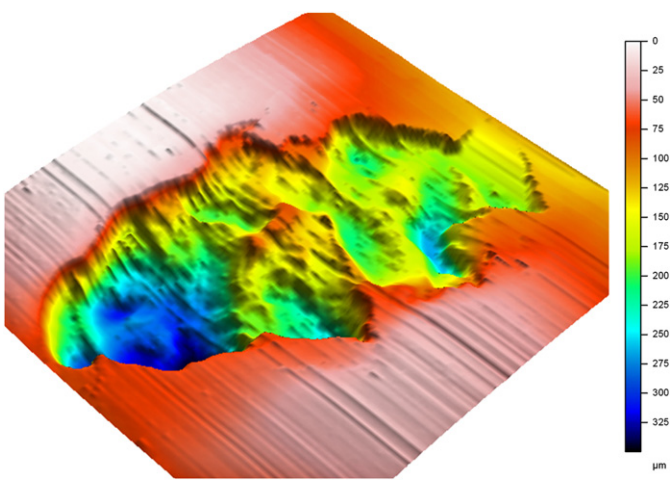

Fig. 10. 3D image of surface spall.

4.3. Effect of surface roughness on rolling contact fatigue life

The rolling contact fatigue life results, referred to the number of stress cycles required to initial spalling of test specimens, are reported in Fig. 11. The results show that RCF life increases as R_a value decreases. Indeed, with a higher level of roughness amplitude (R_a=0.25 μm) the RCF life reaches 0.32 million cycles, whereas with a very low level of roughness amplitude (R_a=0.1 μm), the RCF life reaches 5.2 million cycles. Therefore, high level of roughness amplitude R_a has a very detrimental effect on RCF life.

4.4. Life comparison of precision hard turned vs. ground, and ground followed by honed specimens

In order to evaluate the impact of the precision hard turning process on rolling contact fatigue life of bearing steel components, a quantitative comparison between precision hard turning, grinding, and grinding followed by honing has been performed. The RCF life tests of ground specimen and ground followed by honed specimen were performed under the same conditions of precision hard turned specimens. Moreover, in order to achieve a good comparative analysis, two complementary RCF tests were conducted on other precision hard turning specimens with different R_a values. Fig. 12 reveals that the bearing components achieved 1.2 million cycles with conventional grinding (R_a=0.2 μm) and 3.2 million cycles with grinding followed honing (R_a=0.05 μm). Thus, precision hard turning, which reaches 5.2 million cycles with surface roughness amplitude R_a=0.1 μm, offers 400% longer RCF life than the grinding process and 60% longer RCF life than grinding followed by honing. Whereas the roughness amplitude (R_a=0.05 μm) obtained with grinding followed by honing is clearly lower, precision hard turning offers better RCF life, which may induce better surface integrity. Therefore, the precision hard turning allows us to improve the surface integrity and RCF life of the roller bearing components.

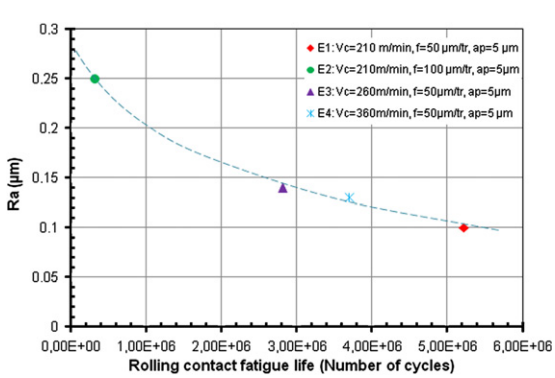

Fig. 11. Effect of surface roughness R_a on rolling contact fatigue of precision hard turning surfaces.

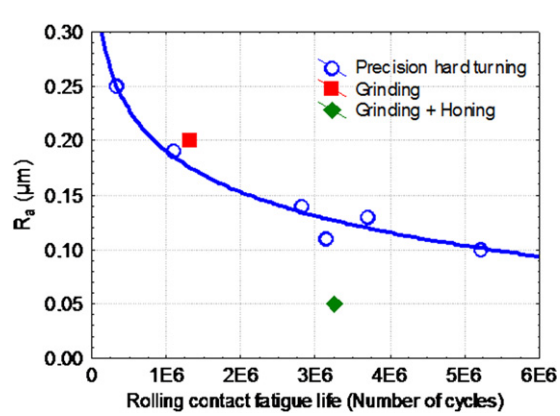

Fig. 12. Life comparison of precision hard turned vs. ground, and ground followed by honed specimen.

Conclusion

This paper investigates the feasibility of the precision hard turning as a finishing process to improve the rolling fatigue life of the bearing steel components.

The results can be summarized as follows:

- Precision hard turning generates homogeneous thicknesses of fine white layer and transition zone. Nanoindentation tests have revealed that the white layer is about 50% harder than the bulk material hardness, and the transition zone is about 30% softer than bulk material.
- RCF life of bearing steel components machined by precision hard turning reached 5.2 (at $R_a = 0.11\ \mu m$) and 0.32 million cycles (at $R_a = 0.25\ \mu m$). Therefore, RCF life increases as the roughness amplitude R_a decreases.
- In comparison with precision hard turning (RCF life reaches 5.2 million cycles for $R_a = 0.11\ \mu m$), the RCF life of the bearing components finished by grinding process reached 1.2 million cycles ($R_a = 0.2\ \mu m$), whereas in grinding followed by honing process it reached 3.2 million cycles ($R_a = 0.05\ \mu m$).

References

[1] König W, Berktold A, Koch KF. Turning versus grinding—a comparison of surface integrity aspects and attainable accuracies. CIRP Annals—Manufacturing Technology 1993;42:39–43.
[2] Klocke F, Brinksmeier E, Weinert K. Capability profile of hard cutting and grinding processes. CIRP Annals—Manufacturing Technology 2005;54:22–45.
[3] Matsumoto Y, Hashimoto F, Lahoti G. Surface integrity generated by precision hard turning. CIRP Annals—Manufacturing Technology 1999;48:59–62.
[4] Novovic D, Dewes RC, Aspinwall DK, Voice W, Bowen P. The effect of machined topography and integrity on fatigue life. International Journal of Machine Tools and Manufacture 2004;44:125–34.
[5] Paulin C, Ville F, Sainsot P, Coulon S, Lubrecht T. Effect of rough surfaces on rolling contact fatigue theoretical and experimental analysis. In: Proceedings of the 30th Leeds–Lyon symposium on tribology, Elsevier tribology and interface engineering series, vol 43, 2003. p. 611–17.
[6] Field M, Kahles JF. The surface integrity of machined and ground high strength steels. DMIC Report 1964;210:54–77.
[7] Hooke CJ, Li KY. Roughness in elastohydrodynamic contacts. Proceedings of the Institution of Mechanical Engineers, Part C:Journal of Mechanical Engineering Science 2010;224:2590–609.
[8] Morales-Espejel GE, Gabelli A, Ioannides E. Micro-geometry lubrication and life ratings of rolling bearings. Proceedings of the Institution of Mechanical Engineers, Part C: Journal of Mechanical Engineering Science 2010;224:2610–26.
[9] Chapkov AD, Colin F, Lubrecht AA. Influence of harmonic surface roughness on the fatigue life of elastohydrodynamic lubricated contacts. Proceedings of the Institution of Mechanical Engineers, Part J: Journal of Engineering Tribology 2006;220:287–94.
[10] Biboulet N, Lubrecht AA, Houpert L. Contact pressure in indented elastohydrodynamic lubrication contacts. Proceedings of the Institution of Mechanical Engineers, Part J:Journal of Engineering Tribology 2008;222:415–21.
[11] Kumar P, Jain SC, Ray S. Study of surface roughness effects in elastohydrodynamic lubrication of rolling line contacts using a deterministic model. Tribology International 2001;34:713–22.
[12] Coulon S, Jubault I, Lubrecht AA. Pressure profiles measured within lubricated contacts in presence of dented surfaces. Comparison with numerical models. Tribology International 2004;37:111–7.
[13] Labiau A, Ville F, Sainsot P, Querlioz E, Lubrecht T. Effect of sinusoidal surface roughness under starved conditions on rolling contact fatigue. Proceedings of the Institution of Mechanical Engineers, Part J: Journal of Engineering Tribology 2008;222:193–200.
[14] Bhadeshia HKDH. Steels for bearings. Progress in Materials Science 2012;57:268–435.
[15] Olver AV. The mechanism of rolling contact fatigue: an update. Proceedings of the Institution of Mechanical Engineers, Part J: Journal of Engineering Tribology 2005;219:313–30.
[16] Liu JY, Tallian TE, McCool JI. Dependence of bearing fatigue life on film thickness to surface roughness ratio. Tribolgy Transaction 1975;18:144–52.
[17] Tallian TE. Failure atlas for hertz contact machine elements. New York: ASME Press; 1992.
[18] Schwach DW, Guo YB. A fundamental study on the impact of surface integrity by hard turning on rolling contact fatigue. International Journal of Fatigue 2006;28:1838–44.
[19] Tonshoff H, Arendt C, Ben Amor R. Cutting of hardened steel. CIRP Annals—Manufacturing Technology 2000;49:547–66.
[20] Griffiths BJ. Mechanisms of white layer generation with reference to machining and deformation processes. Journal of Tribology—Transactions of the ASME 1987;109:525–30.
[21] Akcan S, Shah S, Moylan SP, Chhabra PN, Chandraseksar S, Yang HTY. Formation of white layers in steels by machining and their characteristics. Metallurgical and Materials Transactions A 2002;33:1245–54.
[22] Ramesh A, Melkote SN, Allard L, Riester L, Watkins TR. Analysis of white layers formed in hard turning of AISI 52100 steel. Materials Science and Engineering A 2005;390:88–97.
[23] Smith S, Melkote SN, Lara-curzio E, Watkins TR, Allard L, Riester L. Effect of surface integrity of hard turned AISI 52100 steel on fatigue performance. Materials Science and Engineering A 2007;459:337–46.
[24] Abrao AM, Aspinwall DK. The surface integrity of turned and ground hardened bearing steel. Wear 1996;196:279–84.
[25] König W, Klinger M, Link R. Machining hard materials with geometrically defined, cutting edges—field of applications and limitations. CIRP Annals—Manufacturing Technology 1990;39:61–4.
[26] Oliver WC, Pharr GM. An improved technique for determining hardness and elastic modulus using load and displacement sensing indentation experiments. Journal of Materials Research 1992;7:1564–83.
[27] Oliver WC, Pharr GM. Measurement of hardness and elastic modulus by instrumented indentation: advances in understanding and refinements to methodology. Journal of Materials Research 2004;19:3–20.
[28] Chou YK, Evans CJ. White layers and thermal modelling of hard turned surface. International Journal of Machine Tools and Manufacturing 1999;39:1863–81.
[29] Jouini N, Revel P, Bigerelle M Relevant roughness parameters of precision hard turning surfaces. In: Proceedings of 4th CIRP international conference on high performance cutting, vol 1, 2010, p. 23–32.
[30] Bigerelle M, Gautier A, Iost A. Roughness characteristic length scales of micro-machined surfaces: a multi-scale modeling. Sensors and Actuators B: Chemical 2007;126:126–37.
[31] Najjar D, Bigerelle M, Iost A. The computer-based bootstrap method as a tool to select a relevant surface roughness parameter. Wear 2003;254:450–60.
[32] Bigerelle M, Najjar D, Iost A. Multiscale functional analysis of wear a fractal model of the grinding process. Wear 2005;258:232–9.
[33] Bigerelle M, Hagege B, El Mansori M. Mechanical modelling of micro-scale abrasion in superfinish belt grinding. Tribology International 2008;41: 992–1001.
[34] Bigerelle M, Anselme K, Dufresne E, Hardouin P, Iost A. An unscaled parameter to measure the order of surfaces: a new surface elaboration to increase cells adhesion. Biomolecular Engineering 2002;19:79–83.
[35] Isselin J, Iost A, Golek J, Najjar D, Bigerelle M. Assessment of the constitutive law by inverse methodology: small punch test and hardness. Journal of Nuclear Materials 2006;352:97–106.
[36] Bigerelle M, Iost A. Bootstrap analysis of FCGR, application to the Paris relationship and to lifetime prediction. International Journal of Fatigue 1999;21:299–307.
[37] Bigerelle M, Anselme K. Bootstrap analysis of the relation between initial adhesive events and long-term cellular functions of human osteoblasts cultured on biocompatible metallic substrates. Acta Biomaterialia 2005;1: 499–510.